



Combined removal of diesel soot particulates and NO_x over CeO₂–ZrO₂ mixed oxides

I. Atribak, A. Bueno-López*, A. García-García

Department of Inorganic Chemistry, University of Alicante, Ap. 99 E-03080, Alicante, Spain

ARTICLE INFO

Article history:

Received 17 April 2008

Revised 15 June 2008

Accepted 31 July 2008

Available online 30 August 2008

Keywords:

Catalysed soot oxidation

Ceria

Ce–Zr mixed oxide

Solid solution

Soot

NO_x

Diesel pollution control

ABSTRACT

CeO₂ and Ce–Zr mixed oxides with different Ce:Zr ratios were prepared; characterised by Raman spectroscopy, XRD, TEM, N₂ adsorption at –196 °C, and H₂-TPR; and tested for soot oxidation under NO_x/O₂. Among the different mixed oxides, Ce_{0.76}Zr_{0.24}O₂ provided the best results. Ce_{0.76}Zr_{0.24}O₂ presented greater activity than pure CeO₂ for soot oxidation by NO_x/O₂ when both catalysts were calcined at 500 °C (soot oxidation rates at 500 °C are 14.9 and 11.4 μg_{soot}/s, respectively), and the catalytic activity of CeO₂ decayed significantly with calcination temperature (from 500 to 1000 °C), whereas Ce_{0.76}Zr_{0.24}O₂ presented enhanced thermal stability at temperatures as high as 1000 °C. In addition, Ce_{0.76}Zr_{0.24}O₂ catalysed the reduction of NO_x by soot at around 500 °C more efficiently than CeO₂, thereby contributing to the decreased NO_x emission level. The catalytic activity of CeO₂ and Ce_{0.76}Zr_{0.24}O₂ for soot oxidation by NO_x/O₂ depended on the textural properties (BET area; crystallite size), but other properties of the oxides, such as redox behaviour and/or enhanced lattice oxygen mobility, also played a significant role.

© 2008 Elsevier Inc. All rights reserved.

1. Introduction

Ceria is an important material in the framework of the three-way catalysts (TWCs) used in gasoline automobile catalytic converters for the treatment of exhaust gases [1,2]. One of the key functions of this material is the ability of cerium to switch between the Ce⁴⁺ and Ce³⁺ oxidation states and to incorporate more or less oxygen into their crystal structure depending on various parameters, such as the gaseous atmosphere with which they are in contact, temperature, and pressure [3]. Therefore, early on, ceria played a main role as an oxygen storage component to extend the three-way window on the lean side of stoichiometry by acting as a sink for gas-phase oxygen during rich-to-lean transients in air-to-fuel ratio [1–3]. On the other hand, the oxygen storage component also could promote oxidation of reductants, like CO, during lean-to-rich transients [3]. TWC formulation has undergone significant advances during the past 20 years, mainly using ceria in solid solution with other metal oxides, most notably zirconia [1,4]. The advanced TWC formulations are capable of much higher temperature operation than their predecessors and have dramatically improved long-term emissions performance [2,4].

Adding zirconium to ceria to form a mixed-oxide solution is known to greatly enhance the reducibility of Ce⁴⁺ in the catalyst material. This has generated considerable interest in the Ce–Zr sys-

tem [5–8]. The energetics of the Ce⁴⁺/Ce³⁺ reduction step and the corresponding formation of oxygen vacancies are likely involved [9]. Indeed, fundamental solid-state properties, such as the precise role of structural defects and dopants, the nature of redox reactions to create electronic species (both within the bulk and at the surfaces), and the mechanism of oxygen migration clearly are crucial to gaining insight into these important materials.

The unique features of oxygen storage capacity have made Ce–Zr binary oxides important in numerous catalytic processes besides TWCs, including CO oxidation [10], light hydrocarbon combustion [11,12] and VOC oxidation [13]. The key steps of these reactions are the supply of oxygen by the readily reducible mixed oxide and its reoxidation by oxygen. The Ce–Zr mixed oxides are better catalysts than bare CeO₂, because the partial substitution of Ce⁴⁺ (ionic radii = 0.97 Å) with Zr⁴⁺ (ionic radii = 0.84 Å) leads to deformation of the lattice, improving its oxygen storage capacity, redox properties, and thermal resistance [5–8,14,15].

The important role of the active oxygen generated by CeO₂ in the catalysed oxidation of soot by O₂ also has been reported recently [16]. This oxide is of interest as a catalyst for the regeneration of soot traps fitted in the exhaust of diesel engines [17,18]. Doping of ceria with Zr [19], La [20,21], or Pr [21] has been found to result in more active catalysts for soot oxidation by O₂, but little information has been reported regarding soot combustion under NO_x/O₂ mixtures catalysed by Ce–Zr mixed oxides.

The catalytic behaviour of CeO₂ for soot oxidation in O₂ is not the same than that in the presence of NO_x. A previous study compared the catalytic activity of pure TiO₂, ZrO₂, and CeO₂ for soot

* Corresponding author. Fax: +34 965 90 34 54.

E-mail addresses: atribak@ua.es (I. Atribak), agus@ua.es (A. Bueno-López), a.garcia@ua.es (A. García-García).

oxidation under $\text{NO}_x + \text{O}_2$ mixtures [22] and concluded that CeO_2 's best activity is related to its capacity to accelerate the NO conversion to NO_2 (TiO_2 and ZrO_2 do not catalyse this reaction), NO_2 being much more oxidizing than NO and O_2 [23]. Rare earth (Sm, Y, La, or Pr)-doped ceria catalysts also have been studied for soot oxidation by NO_x/O_2 ; La and Pr doping enhanced ceria activity and stability, whereas Sm and Y did not [24,25].

CeO_2 has been reported to catalyse the reduction of NO_x by soot, removing both diesel pollutants (soot and NO_x) simultaneously [22]. Pisarello et al. [26] studied the simultaneous removal of NO_x and soot with catalysts containing Co, K, and/or Ba supported on MgO , La_2O_3 , and CeO_2 and concluded that CeO_2 supplied the necessary oxygen for the redox mechanism that occurs during the reaction.

The aim of the present work was to study the catalytic performance of Ce–Zr mixed oxides for the removal of soot under simulated diesel exhaust conditions in a gas flow containing O_2 and NO_x . Special attention was given to the simultaneous removal of NO_x . The catalytic activity of the Ce–Zr mixed oxides was compared with that of pure CeO_2 , and the thermal stability of the pure and mixed oxides was studied in depth, because thermal stability is a key requirement for the application of these materials in an actual soot trap.

2. Experimental

2.1. Catalyst preparation

Ce–Zr mixed oxides with different metal ratios were prepared through a co-precipitation route. The required amounts of $\text{ZrO}(\text{NO}_3)_2 \cdot 6\text{H}_2\text{O}$ and/or $\text{Ce}(\text{NO}_3)_3 \cdot 6\text{H}_2\text{O}$ (supplied by Aldrich) were dissolved in water, and the hydroxides were precipitated by dropping an ammonia solution to maintain the pH at about 9. The precipitates were dried at 90°C in air overnight and calcined in air for 3 h at different temperatures in the range of 500 – 1000°C . Pure CeO_2 and ZrO_2 also were prepared following the same procedure. The CeO_2 and ZrO_2 pure oxides are designated CeO_2 -T and ZrO_2 -T, respectively, and the Ce–Zr mixed oxides are designated $\text{Ce}_x\text{Zr}_{1-x}\text{O}_2$ -T (formal composition, $0 < x < 1$), where x is the molar fraction of CeO_2 in the mixed oxides and T is the calcination temperature.

2.2. Catalytic tests

The catalytic tests were performed in a tubular quartz reactor coupled to specific NDIR-UV gas analysers for CO, CO_2 , NO, NO_2 , and O_2 monitoring. First, 20 mg of soot and 80 mg of the selected catalyst were mixed under so-called “loose contact” conditions [27] and diluted with SiC to avoid pressure drop and favour heat transfer. The gas mixture comprised 500 ppm NO_x , 5% O_2 , and balance N_2 , and the gas flow was fixed at 500 ml/min ($\text{GHSV} = 30,000 \text{ h}^{-1}$).

Two types of experiments were carried out. In temperature-programmed reactions, the gas mixture was fed to the reactor, and then the temperature was increased from room temperature up to 700°C at a ramp rate of $10^\circ\text{C}/\text{min}$. In isothermal reactions, the temperature was raised from room temperature up to 500°C , with the soot-catalyst mixture maintained in N_2 flow, and then the N_2 flow was replaced by the reaction gas mixture. These experiments were conducted until total conversion of soot occurred.

The model soot used was a carbon black from Degussa (Printex U), with $<0.1\%$ ash content, 5% volatile matter, 92.2% C, 0.6% H, 0.2% N, and 0.4% S. Soot conversion profiles were determined from CO and CO_2 evolved, and the selectivity of the different catalysts toward CO emission was determined by

$$\text{CO}/\text{CO}_x (\%) = 100\text{CO}/(\text{CO} + \text{CO}_2).$$

Blank experiments were performed under the aforementioned experimental conditions but without soot, that is, using only catalyst.

2.3. Characterisation techniques

The textural properties were determined by multipoint N_2 adsorption at -196°C using an automatic Quantachrome Autosorb-6B instrument. Data were treated in accordance with the BET method. The samples had been previously degassed for 4 h at 250°C under vacuum.

A JEOL JEM-2010 microscope was used to obtain TEM images of the catalysts. Few droplets of an ultrasonically dispersed suspension of each catalyst in ethanol were placed in a grid and dried at ambient conditions for TEM characterisation.

Raman spectra of the catalysts were recorded in a Bruker RFS 100/S Fourier transform Raman spectrometer with a variable power Nd:YAG laser source (1064 nm). A total of 64 scans at 85 mW laser power (70 mW on the sample) were recorded, and no heating of the sample was observed under these conditions.

X-ray diffractograms of the catalysts were recorded in a Bruker D8 advance diffractometer, using $\text{CuK}\alpha$ radiation. Spectra were registered between 10° and 80° (2θ) with a step of 0.02° and a time per step of 3 s. The average crystal size (D) of the catalysts was determined using the equations of Scherrer and Williamson–Hall. Scherrer's equation is

$$D = \frac{K \cdot \lambda}{\beta \cdot \cos \theta},$$

where λ is the wavelength of the radiation used ($\lambda = 0.15418 \text{ nm}$ for $\text{CuK}\alpha$); β is the full width at half maximum of the diffraction peak considered (111); K is a shape factor, taken to be 0.9 (with 1 being a perfect sphere); and θ is the diffraction angle at which the peak appears.

Estimating the crystal size of doped oxides presents some problems, because the introduction of foreign cations within the lattice deforms the structure and affects the β values. The Williamson–Hall equation separates the effects of size and strain in the crystals and is more convenient for estimating crystal size of mixed oxides,

$$\beta_{\text{Total}} = \beta_{\text{Size}} + \beta_{\text{Strain}} = \frac{0.9\lambda}{D \cos \theta} + \frac{4(\Delta d) \sin \theta}{d \cos \theta},$$

where β_{Total} is the full width half maximum of the XRD peak and Δd is the difference of the d spacing corresponding to a typical peak. A plot of $\beta_{\text{Total}} \cos \theta$ against $4 \sin \theta$ yields the average crystal size from the intercept value. Despite the improvement introduced by the Williamson–Hall equation over Scherrer's equation, the crystal sizes estimated for the Ce–Zr mixed oxides prepared in this study must be considered semiquantitative values, because some of the data obtained are not fully consistent with the BET areas estimated by N_2 adsorption.

The redox behaviour of the catalysts was examined by H_2 -TPR in a Micromeritics Pulse ChemiSorb 2705 device consisting of a tubular quartz reactor coupled to a TCD detector to monitor H_2 consumption. The reducing gas used was 5% H_2 in He. The temperature range explored was from room temperature to 900°C , and the heating rate was $10^\circ\text{C}/\text{min}$.

3. Results and discussion

3.1. Temperature-programmed reactions: Soot oxidation

Fig. 1 compares the catalytic activity of two series of Ce–Zr mixed oxides, calcined at 500 and 1000°C , respectively. The temperature required to convert 50% of the soot (T50%) in each experiment is plotted as a function of the Zr molar fraction of the catalysts used. The T50% temperature for the uncatalysed reaction

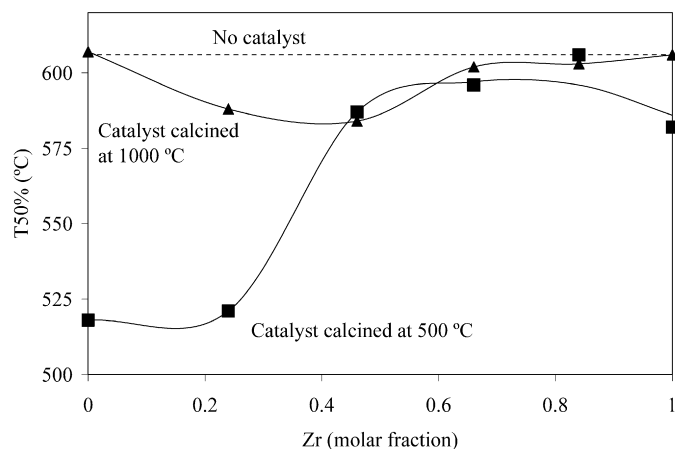


Fig. 1. Effect of the Ce:Zr ratio on soot combustion.

was 606 °C under the experimental conditions used here, and most of the samples decreased this temperature. Among the catalysts calcined at 500 °C, CeO_2 -500 and $\text{Ce}_{0.76}\text{Zr}_{0.24}\text{O}_2$ -500 exhibited the best performance, and increasing the Zr loading above this molar fraction had a negative effect on the activity because of the lower amount of Ce available. This is consistent with the fact that the couple $\text{Ce}^{3+}/\text{Ce}^{4+}$ is the responsible of the catalytic activity for soot oxidation of CeO_2 -based catalysts. The same activity trend has been reported previously [19] for $\text{Ce}_x\text{Zr}_{1-x}\text{O}_2$ -catalysed soot combustion in air ($0 \leq x \leq 1.0$ composition; catalysts calcined at 500 °C; soot and catalyst in tight contact), where the highest activity was obtained with cerium-rich mixtures (with $x = 1.0$ and $x = 0.75$). The arguments provided [19] to explain these results were that cerium-rich samples have greater availability of surface Ce^{4+} sites and that these materials (solid solutions) have a better ability to donate oxygen for soot oxidation. The highest catalytic activity of $\text{Ce}_x\text{Zr}_{1-x}\text{O}_2$ mixed oxides with $x \sim 0.75$, compared with higher zirconium loading, also has been reported for the selective catalytic reduction of NO_x by hydrocarbons [28].

The activity of the catalysts decreased when they were calcined at 1000 °C (Fig. 1), and the degree of thermal deactivation depended on their composition. Pure CeO_2 and pure ZrO_2 became inactive when calcined at 1000 °C. $\text{Ce}_{0.76}\text{Zr}_{0.24}\text{O}_2$ exhibited a partial decrease in activity after calcination at 1000 °C. Ce–Zr mixtures with a Zr molar fraction >0.24 calcined at 1000 °C maintained the poor activity of the counterpart catalysts calcined at 500 °C. The thermal stability of CeO_2 is a critical aspect of its application in catalysis, as was seen in TWCs, where the low stability of the pure CeO_2 used in early formulations required the development of advanced CeO_2 -based materials with enhanced thermal resistance [2]. Pijolat et al. [29] investigated the effect of foreign cation doping on the thermal stability of CeO_2 and concluded that among the different cations investigated (Th^{4+} , Zr^{4+} , Si^{4+} , La^{3+} , Y^{3+} , Sc^{3+} , Al^{3+} , Ca^{2+} , and Mg^{2+}), those with ionic radii smaller than that of Ce^{4+} effectively stabilised the CeO_2 against sintering. This observation is consistent with the improved thermal resistance of $\text{Ce}_{0.76}\text{Zr}_{0.24}\text{O}_2$ compared with pure CeO_2 .

Another feature of the soot oxidation catalysts that must be analysed together with the decrease in soot oxidation temperature is the production of CO_2 and/or CO as a soot gasification product, with CO_2 being the desired gas product because of CO 's high toxicity. A general feature of carbon combustion reactions is that the CO production increases and CO_2 production decreases with increasing temperature. Therefore, on one hand, when a catalyst decreases the soot combustion temperature, CO_2 formation is favoured and, on the other hand, CeO_2 -based catalysts are effective for catalysing the oxidation of CO to CO_2 [2]. Both catalyst properties determine

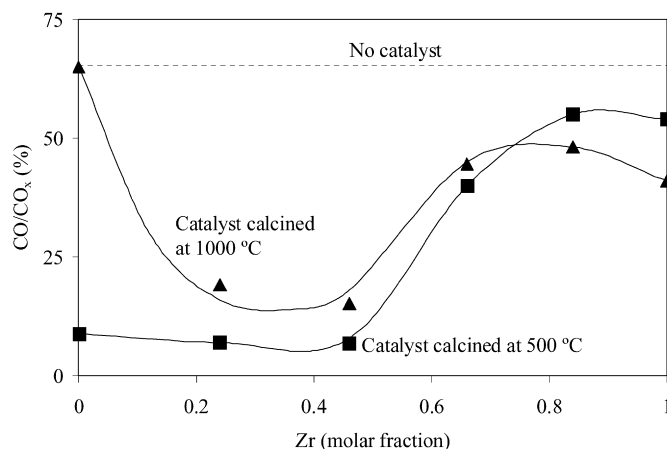


Fig. 2. Effect of the Ce:Zr ratio on CO emission.

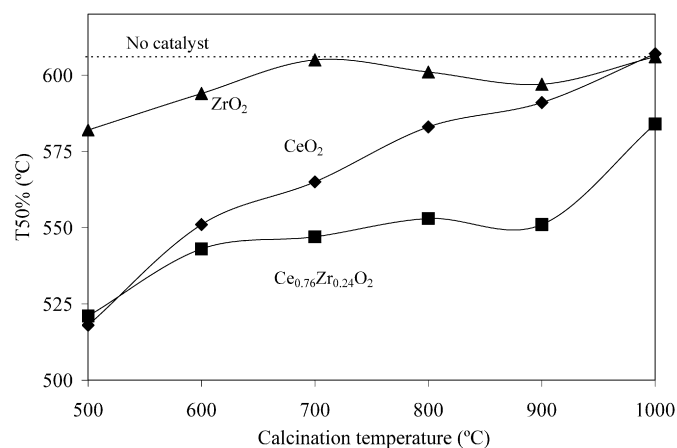


Fig. 3. Effect of the calcination temperature of catalyst on soot combustion.

the amount of CO and CO_2 yielded during the catalysed soot oxidation reactions.

Fig. 2 shows the percentage of CO evolved during the experiments performed with the series of catalysts calcined at 500 and 1000 °C. The uncatalysed reaction yielded 65% CO ; all of the catalysts except CeO_2 -1000 decreased this value. The best results were obtained with CeO_2 -500 and with Ce–Zr mixtures with a Zr molar fraction ≤ 0.46 . The calcination temperature of the Ce–Zr mixtures had only a minor effect on CO selectivity.

To summarise the findings shown in Figs. 1 and 2, the best formulation obtained was $\text{Ce}_{0.76}\text{Zr}_{0.24}\text{O}_2$. This material exhibited the same activity and selectivity for CO_2 formation as pure CeO_2 when both catalysts were calcined at 500 °C but showed enhanced thermal stability, maintaining part of its activity for soot oxidation and selectivity for CO_2 formation after calcination at temperatures as high as 1000 °C. This conclusion is in agreement with that reached by Aneghi et al. [19] for CeO_2 - and $\text{Ce}_{0.75}\text{Zr}_{0.25}\text{O}_2$ -catalysed soot combustion in air (with catalysts calcined at 500 and 800 °C). These authors concluded that the main difference between pure ceria and cerium–zirconium solid solution is related to the stability after calcination.

We studied the effect of calcination temperature on the catalytic activity of CeO_2 , ZrO_2 , and $\text{Ce}_{0.76}\text{Zr}_{0.24}\text{O}_2$ in more detail at 500–1000 °C. Figs. 3 and 4 show the results obtained for activity and selectivity toward CO_2 formation, respectively. In all series of catalysts, the catalytic activity for soot oxidation (Fig. 3) decreased with calcination temperature. As expected, ZrO_2 had very poor activity regardless of calcination temperature [22]. CeO_2 and $\text{Ce}_{0.76}\text{Zr}_{0.24}\text{O}_2$ showed similar activity when catalysts were calcined

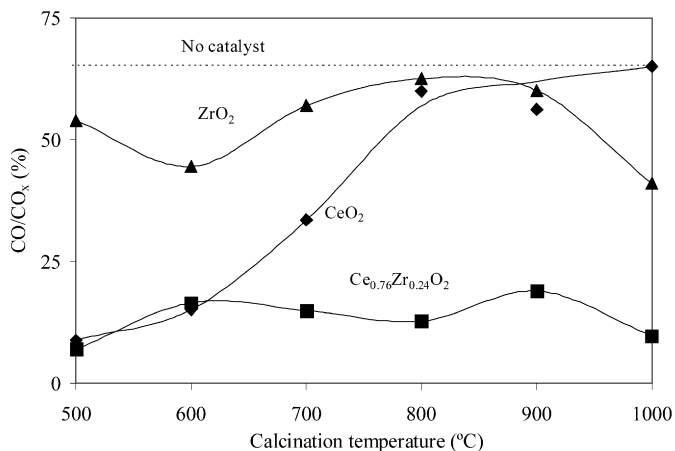


Fig. 4. Effect of the calcination temperature of catalyst on CO emission.

at 500 °C, but not at higher calcination temperatures. In general, the $\text{Ce}_{0.76}\text{Zr}_{0.24}\text{O}_2$ catalysts were more active than their counterpart CeO_2 catalysts. The activity of CeO_2 decreased quite monotonically from 500 to 1000 °C, with CeO_2 -1000 not active at all. In contrast, the activity of $\text{Ce}_{0.76}\text{Zr}_{0.24}\text{O}_2$ for soot oxidation clearly decreased between 500 and 600 °C (with T50% increasing from 521 °C to 543 °C, respectively) but was not modified significantly further until 900 °C, indicating very high thermal stability within the range of 600–900 °C. The activity of $\text{Ce}_{0.76}\text{Zr}_{0.24}\text{O}_2$ decreased further only between 900 and 1000 °C, but some activity remained.

The effect of calcination temperature on the selectivity toward CO_2 formation was found to depend significantly on the catalyst formulation (Fig. 4). Regardless of the calcination temperature, $\text{Ce}_{0.76}\text{Zr}_{0.24}\text{O}_2$ yielded a low CO percentage ($13 \pm 6\%$) and ZrO_2 yielded a high CO percentage ($53 \pm 12\%$). CO formation during CeO_2 -catalysed soot oxidation increased slightly with catalysts calcined between 500 and 600 °C but increased dramatically between 600 and 800 °C, almost reaching the CO percentage yielded during the uncatalysed reaction. These results confirm that $\text{Ce}_{0.76}\text{Zr}_{0.24}\text{O}_2$ was the best among the different formulations studied, based on its activity for soot oxidation, high thermal stability, and high selectivity toward CO_2 formation as a soot oxidation product.

3.2. Temperature-programmed reactions: NO_x elimination

The elimination of NO_x during the TPRs also depended on the catalyst used, as shown in Fig. 5a for catalysts calcined at 500 °C. This type of profile was previously studied in detail for pure CeO_2 catalysts [22]. Considering as an example the NO_x elimination profile obtained with $\text{Ce}_{0.76}\text{Zr}_{0.24}\text{O}_2$ (see Fig. 5a), three different processes can be distinguished between 225 °C and 700 °C: The maximum NO_x elimination level was reached at 400 °C, and two shoulders appeared at higher temperatures, around 500 and 600 °C. This profile suggests three different NO_x elimination pathways. The shape of the NO_x elimination curves depends on the catalyst used; in other words, the relative importance of each NO_x elimination pathway differs for each catalyst. The three NO_x elimination profiles are as follows:

- NO_x elimination around 400 °C and lower temperatures. The elimination of NO_x is mainly attributed to NO_x chemisorption on the catalysts, as supported by the blank experiments (without soot) shown in Fig. 6a. NO_x chemisorption on Ce–Zr mixtures (Fig. 5a) at around 400 °C decreased by increasing the Zr molar fraction, because NO_x chemisorption occurred on Ce but not on Zr [22]. The NO_x elimination levels reached at 400 °C by $\text{Ce}_{0.76}\text{Zr}_{0.24}\text{O}_2$ -500 and CeO_2 -500 (Fig. 5a) differed slightly,

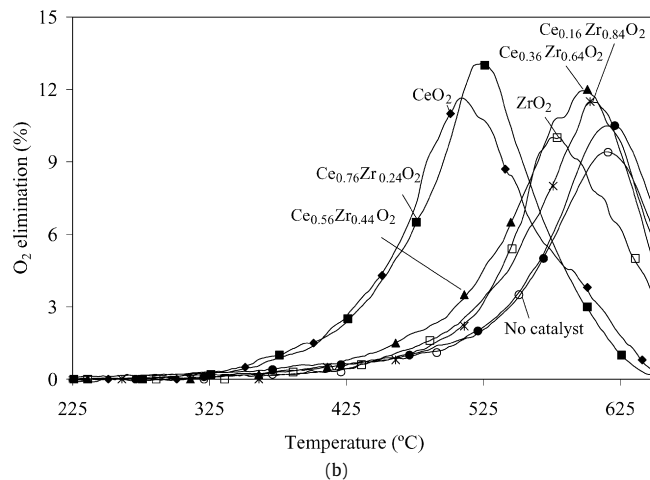
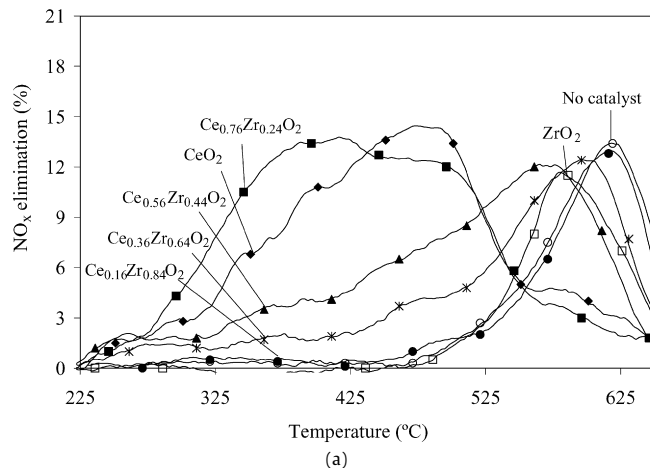


Fig. 5. Effect of the Ce:Zr ratio on: (a) NO_x elimination and (b) O_2 elimination (catalysts calcined at 500 °C).

whereas the NO_x chemisorption in both catalysts observed in blank experiments (Fig. 6a) were the same. This suggests a certain contribution of another NO_x elimination pathway (NO_x reduction by soot), in addition to NO_x chemisorption.

- NO_x elimination at around 500 °C. The elimination of NO_x at around this temperature can be attributed in part to the catalysed soot– NO_x reaction, with NO_x consumed due to reduction by soot. This is the most interesting NO_x elimination pathway, because it allows the simultaneous abatement of NO_x and soot by the reaction of both pollutants with each other. The formation of N_2O as a reaction product was not detected in other experiments followed by gas chromatography [22]. O_2 also was converted at around 500 °C due to soot combustion, as shown in Fig. 5b. As mentioned in the previous section, the catalytic activity for soot oxidation of the series of catalysts calcined at 500 °C decreased with increasing Zr molar fraction (Fig. 1), with $\text{Ce}_{0.76}\text{Zr}_{0.24}\text{O}_2$ -500 being the most active Ce–Zr mixture.
- NO_x elimination at around 600 °C. The elimination of NO_x at around this temperature can be attributed mainly to the uncatalysed soot– NO_x reaction, occurring along with the soot– O_2 reaction (see Fig. 5b). As shown in Fig. 5a, this is the only NO_x elimination pathway for the least active catalysts (ZrO_2 -500, $\text{Ce}_{0.16}\text{Zr}_{0.84}\text{O}_2$ -500, and $\text{Ce}_{0.36}\text{Zr}_{0.64}\text{O}_2$ -500).

A key factor influencing the catalysed soot oxidation reactions in the presence of NO_x is NO_2 production by the different catalysts. Fig. 6b plots the NO_2 percentage (on the basis of $\text{NO} + \text{NO}_2$) as a function of temperature for blank experiments. Above 275 °C,

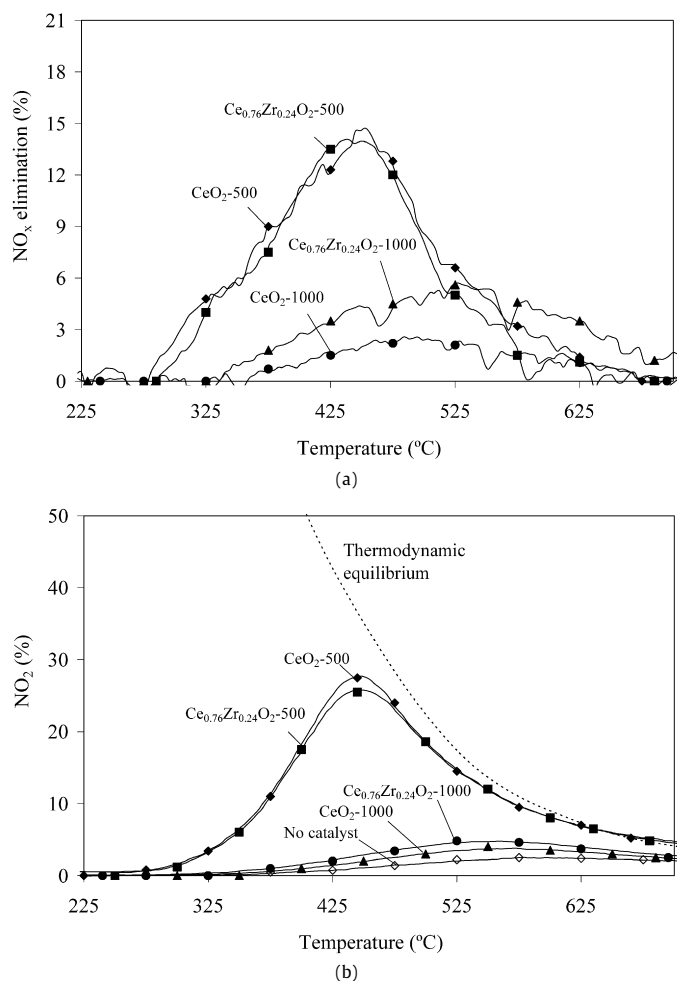


Fig. 6. Blank experiments (without soot): (a) NO_x elimination and (b) NO_2 formation.

$\text{Ce}_{0.76}\text{Zr}_{0.24}\text{O}_2-500$ and CeO_2-500 catalysed the oxidation of NO to NO_2 , reaching a maximum NO_2 level corresponding to the thermodynamic equilibrium at 450°C and decreasing at higher temperatures following thermodynamics. In contrast, the catalysts calcined at 1000°C were not effective for converting NO into NO_2 , consistent with the lower activity of the $\text{Ce}_{0.76}\text{Zr}_{0.24}\text{O}_2-1000$ and CeO_2-1000 samples for soot oxidation compared with the counterpart samples calcined at 500°C . It is well established [30] that the catalytic activity for soot oxidation of ceria-based catalysts under NO_x mixtures is related to these catalysts' ability to accelerate NO_2 production, with NO_2 being more oxidizing than NO and O_2 .

We also studied the effect of the calcination temperature of CeO_2 and $\text{Ce}_{0.76}\text{Zr}_{0.24}\text{O}_2$ on these catalysts' NO_x elimination capacity; the curves obtained during the corresponding TPRs are shown in Figs. 7a and 7b, respectively. As shown in Fig. 7a, the amount of NO_x removed below 500°C was decreased with calcination temperature, with a dramatic decrease seen from CeO_2-600 to CeO_2-700 . Removal of NO_x through the uncatalysed reaction (at around 600°C) was the main NO_x elimination pathway for CeO_2 calcined at 800°C and higher.

The behaviour of the $\text{Ce}_{0.76}\text{Zr}_{0.24}\text{O}_2$ -series (Fig. 7b) differed from that of the CeO_2 series (Fig. 7a). $\text{Ce}_{0.76}\text{Zr}_{0.24}\text{O}_2$ sustained a gradual decrease in NO_x removal capacity, and only the $\text{Ce}_{0.76}\text{Zr}_{0.24}\text{O}_2-1000$ sample exhibited a NO_x profile ascribed solely to the uncatalysed NO_x -soot reaction. The NO_x elimination profiles indicate that $\text{Ce}_{0.76}\text{Zr}_{0.24}\text{O}_2$ is the best formulation among those studied, because it demonstrated the best performance among the

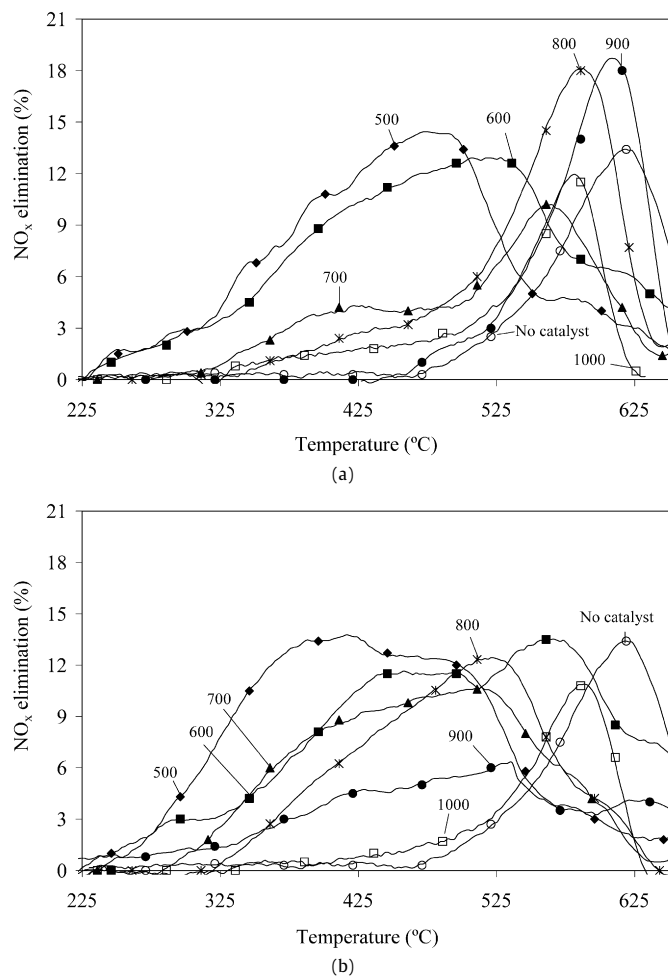


Fig. 7. Effect of the calcination temperature of catalyst on NO_x elimination: (a) CeO_2 -series and (b) $\text{Ce}_{0.76}\text{Zr}_{0.24}\text{O}_2$ -series.

Table 1

Data estimated from isothermal reactions at 500°C

Catalyst	CO/ CO_x (%)	Time for 75% soot conversion (min)	Average soot oxidation rate ($\mu\text{g}_{\text{soot}}/\text{s}$)
CeO_2-500	2.1	24	11.4
CeO_2-1000	11.3	172	1.2
$\text{Ce}_{0.76}\text{Zr}_{0.24}\text{O}_2-500$	3.5	19	14.9
$\text{Ce}_{0.76}\text{Zr}_{0.24}\text{O}_2-1000$	36.8	62	4.1

different catalysts tested and showed enhanced thermal stability with regard to bare CeO_2 .

3.3. Isothermal reactions at 500°C

As described earlier, the TPR results indicate that some of the catalysts tested are able to promote the soot- NO_x reaction at around 500°C , thereby allowing the simultaneous removal of both NO_x and soot. Considering the best performance of $\text{Ce}_{0.76}\text{Zr}_{0.24}\text{O}_2$, its catalytic activity was tested under isothermal conditions at 500°C and was compared with that of bare CeO_2 . In both cases, catalysts calcined at 500 and 1000°C were tested. Fig. 8a shows the soot oxidation rates, expressed per gram of soot remaining in the reactor, and Fig. 8b shows the corresponding NO_x elimination profiles. Table 1 compiles the average soot oxidation rates estimated from isothermal experiments at 500°C , as well as the percentage of CO evolved during the experiments and the time required for 75% soot conversion to $\text{CO} + \text{CO}_2$. Of note, the un-

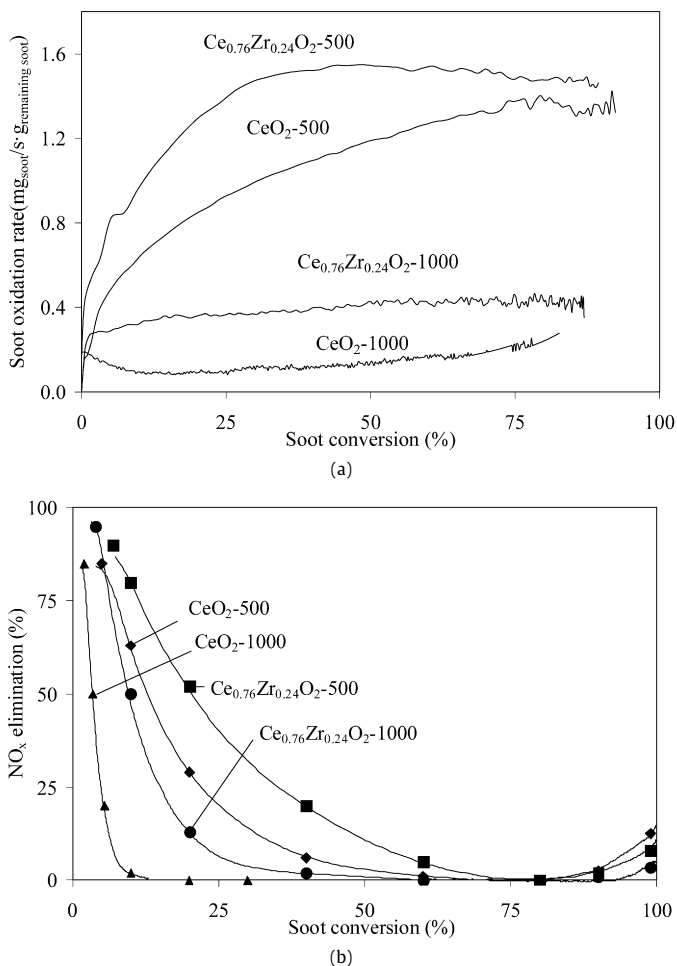


Fig. 8. Isothermal reactions at 500 °C: (a) soot oxidation rate and (b) NO_x elimination. (The units of soot oxidation rate are mg of soot converted per second and gram of soot remaining in the reactor.)

catalysed soot oxidation at 500 °C did not occur under these experimental conditions.

Ce_{0.76}Zr_{0.24}O₂-500 was the most active catalyst for soot oxidation (Fig. 8a) and NO_x reduction (Fig. 8b). The soot oxidation rate during the Ce_{0.76}Zr_{0.24}O₂-500-catalysed experiment rose with soot conversion until about 25% of conversion, which can be attributed to an increased number of active sites for oxygen chemisorption on the soot surface as a result of its progressive oxidation [31,32]. After a certain conversion, the steady state was reached, and a constant rate was maintained. As Table 1 shows, the main reaction product was CO₂, mainly for catalysts calcined at 500 °C, with very low CO emissions (according to TPR results). The reduction of NO_x (Fig. 8b) decreased progressively with soot conversion, as expected because less reductant was available, and NO_x elimination was null after about 75% soot conversion. But a small amount of NO_x was further eliminated once the soot was almost completely consumed, and the NO_x elimination profiles rose slightly at the end of the experiment. This phenomenon was attributed to the chemisorption of NO_x on the catalyst [22]. If soot were available (in Fig. 8, <75% soot conversion for Ce_{0.76}Zr_{0.24}O₂-500), then the reaction of NO_x (mainly NO₂) with soot would be preferable to the storage of NO_x on the catalyst; but once soot were not available (>75% soot conversion), NO_x chemisorption on the catalyst would take place, being the only possible NO_x elimination pathway.

The calcination temperature of the catalyst diminished the catalyst activity, and the soot oxidation rate (Fig. 8a) in steady-state conditions was about threefold lower with Ce_{0.76}Zr_{0.24}O₂-

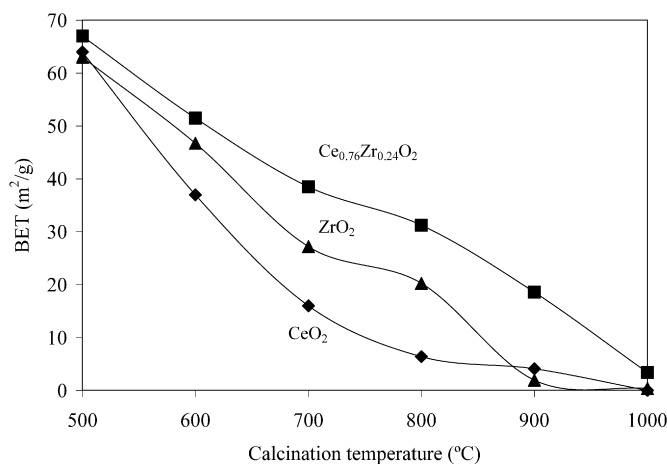


Fig. 9. BET surface areas in terms of calcination temperature of catalysts.

1000 compared with Ce_{0.76}Zr_{0.24}O₂-500. Under our experimental conditions, 75% of the soot used in the experiments was burnt off after 19 min with Ce_{0.76}Zr_{0.24}O₂-500 and after 62 min with Ce_{0.76}Zr_{0.24}O₂-1000. The practical implication of this result is that regeneration of a DPF loaded with Ce_{0.76}Zr_{0.24}O₂-1000 would take about three times longer than regeneration of the same filter loaded with Ce_{0.76}Zr_{0.24}O₂-500. The activity of CeO₂-500 also decreased after calcination at 1000 °C, but in this case the calcination temperature had a dramatic effect. It took 172 min for CeO₂-1000 to convert 75% of the soot used in the experiment, compared with 24 min for CeO₂-500. Because thermal ageing of the catalyst can occur in a real filter, thermally stable active phases are required, and Ce_{0.76}Zr_{0.24}O₂ is preferable to pure CeO₂. In addition, the activity of CeO₂-500 for soot oxidation and NO_x reduction under isothermal conditions at 500 °C was lower than that of Ce_{0.76}Zr_{0.24}O₂-500 (Fig. 8). These differences were not detected in the transient conditions of the TPRs (Figs. 1 and 3), indicating the importance of performing experiments under isothermal conditions, which also provide a more realistic picture of the catalytic behaviour under real conditions.

3.4. Study of the catalytic activity decay due to thermal ageing

The thermal deactivation of CeO₂ and Ce_{0.76}Zr_{0.24}O₂ was studied, and their BET surface areas are shown as a function of the calcination temperature in Fig. 9. The BET surface areas of the samples calcined at 500 °C were approximately similar (~65 m²/g), and the surface areas of all of the oxides decreased significantly with calcination temperature. Ce_{0.76}Zr_{0.24}O₂ exhibited much better thermal resistance than pure CeO₂, because of the stabilising role of Zr. In this type of mixed oxide, the BET value is related to the external surface area of the particles, with high surface area meaning small particle size and vice versa. The TEM pictures shown in Fig. 10 are in agreement with this argument as well as with the crystal sizes determined from XRD by the Scherrer and Williamson-Hall equations (Table 2). In the TEM pictures, CeO₂-500 and Ce_{0.76}Zr_{0.24}O₂-500 appear as quite homogeneous agglomerations of small particles with particle sizes of ca. 10–20 nm, consistent with the crystal sizes determined from the Williamson-Hall equation (22 and 21 nm, respectively). After calcination at 1000 °C, the CeO₂ particles grew due to thermal sintering, forming particles larger than 100 nm (Fig. 10b), whereas Ce_{0.76}Zr_{0.24}O₂-1000 maintained smaller particles of around 20–30 nm (Fig. 10d). Along this line, the Williamson-Hall equation (Table 2) estimated crystal sizes of 107 nm for CeO₂-1000 and 65 nm for Ce_{0.76}Zr_{0.24}O₂-1000.

The structural characterisation of CeO₂ and Ce_{0.76}Zr_{0.24}O₂ samples was carried out by XRD and Raman spectroscopy (Figs. 11

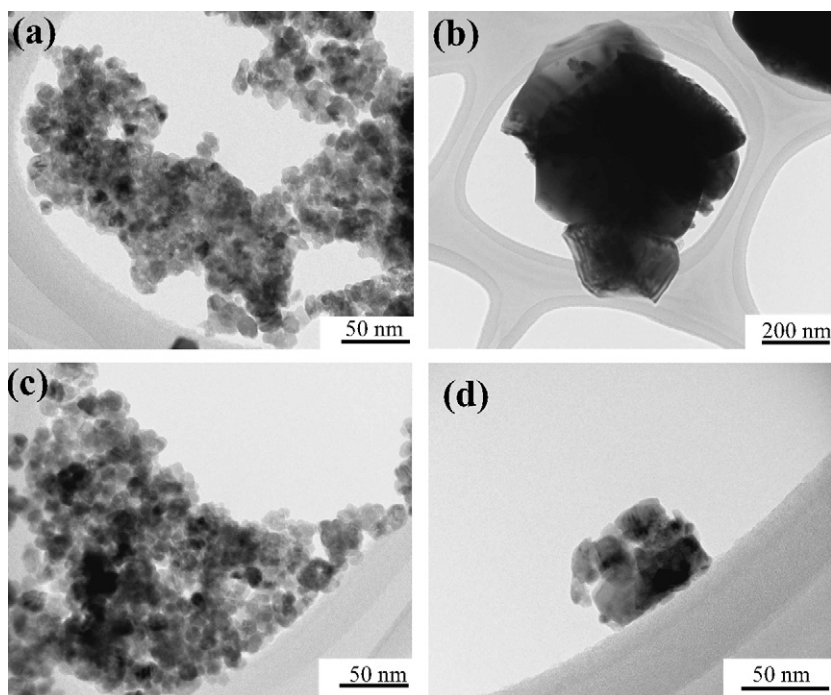
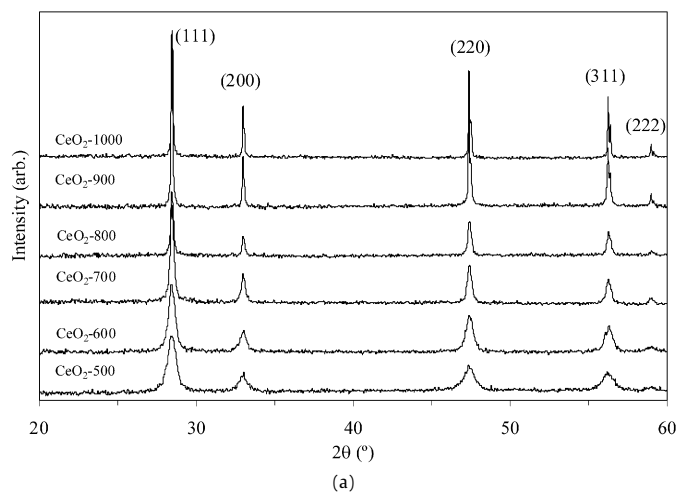
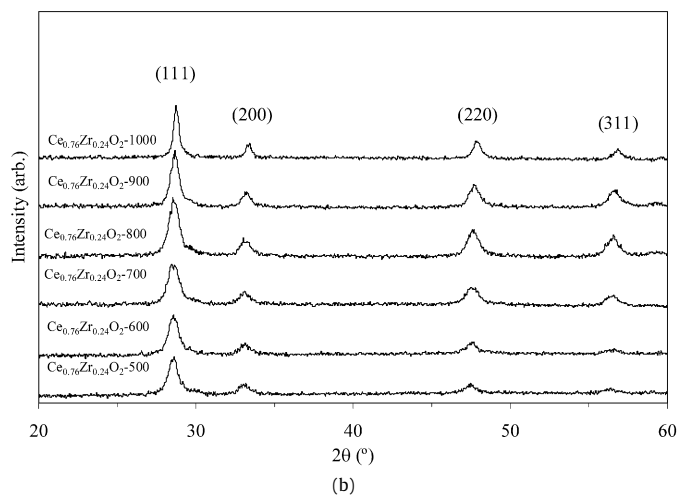


Fig. 10. TEM images: (a) CeO_2 -500, (b) CeO_2 -1000, (c) $\text{Ce}_{0.76}\text{Zr}_{0.24}\text{O}_2$ -500, (d) $\text{Ce}_{0.76}\text{Zr}_{0.24}\text{O}_2$ -1000.

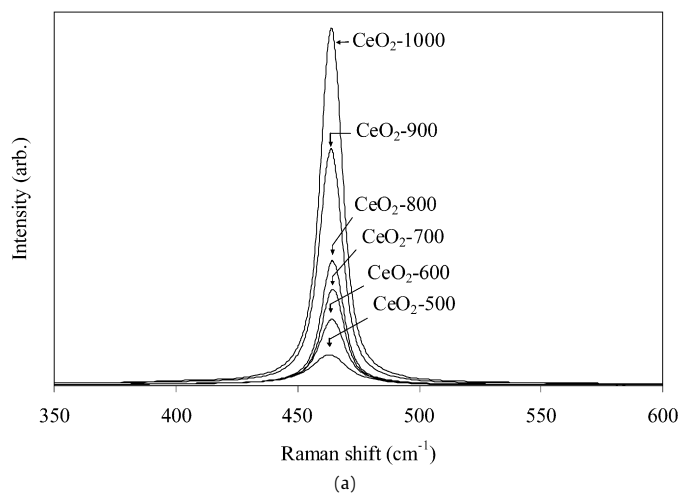


(a)

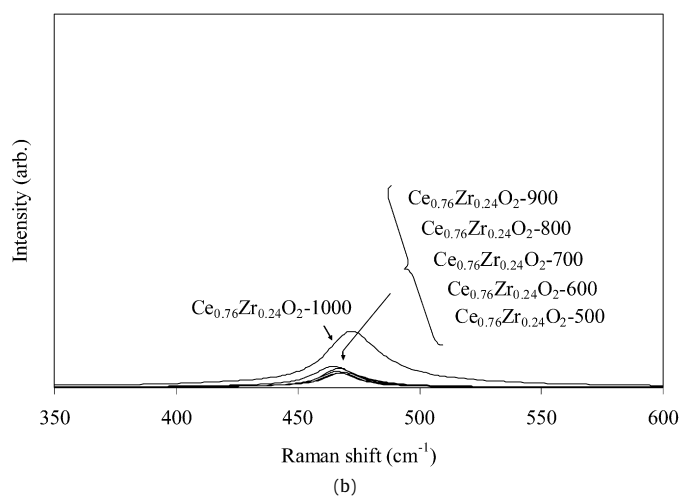


(b)

Fig. 11. XRD characterisation of catalysts: (a) CeO_2 -series and (b) $\text{Ce}_{0.76}\text{Zr}_{0.24}\text{O}_2$ -series.



(a)



(b)

Fig. 12. Raman characterisation of catalysts: (a) CeO_2 -series and (b) $\text{Ce}_{0.76}\text{Zr}_{0.24}\text{O}_2$ -series.

Table 2
Crystal sizes determined from XRD

	Crystal size with Williamson–Hall's equation (nm)	Crystal size with Scherrer's equation (nm)
CeO ₂ -500	22	14
CeO ₂ -600	22	18
CeO ₂ -700	46	32
CeO ₂ -800	63	39
CeO ₂ -900	116	58
CeO ₂ -1000	107	55
Ce _{0.76} Zr _{0.24} O ₂ -500	10	11
Ce _{0.76} Zr _{0.24} O ₂ -600	21	13
Ce _{0.76} Zr _{0.24} O ₂ -700	20	9
Ce _{0.76} Zr _{0.24} O ₂ -800	17	12
Ce _{0.76} Zr _{0.24} O ₂ -900	19	13
Ce _{0.76} Zr _{0.24} O ₂ -1000	65	22

and 12, respectively). All of the diffractograms in Figs. 11a and 11b show the main reflections typical of a fluorite-structured material, with fcc unit cells at 28.5, 33.1, 47.6, and 56.5°, corresponding to the (111), (200), (220), and (311) planes [33]. XRD revealed no evidence of phase segregation for the Ce–Zr mixed oxide (Fig. 11b), with no characteristic ZrO₂ peaks. Some degree of inhomogeneous distribution of cerium and zirconium cannot be ruled out, however, as we discuss next in the context of H₂-TPR characterisation.

Incorporation of Zr into the fluorite structure of CeO₂ caused lattice deformation. At the same calcination temperature, the intensity of the CeO₂ peaks was greater than that of the counterpart Ce_{0.76}Zr_{0.24}O₂ mixed oxide. This is a consequence of the better arrangement of the atoms into the framework of pure CeO₂ and the decreased number of lattice defects. The effect of calcination temperature is clearly shown in Fig. 11a. With increasing calcination temperature, the peaks of CeO₂ narrowed. This is related to an increase in crystal size, which is consistent with BET and TEM characterisation, and also with the negative effect of temperature on the catalytic activity of CeO₂. The same effect of temperature can be seen in the patterns in Fig. 11b but to a lesser extent, in agreement with the greater thermal stability of the Ce–Zr mixed oxide.

Raman characterisation supports the XRD findings. All of the CeO₂ and Ce_{0.76}Zr_{0.24}O₂ samples (Figs. 12a and 12b) exhibited the typical structure of CeO₂, with the main band at 460 cm⁻¹ attributed to the only allowed Raman mode (F_{2g}) of a fluorite-type structure [34,35]. The Raman spectra of these fluorite-type oxide structures are dominated by oxygen lattice vibrations and are sensitive to the crystalline symmetry [36]. The presence of Zr⁴⁺ in the CeO₂ lattice deformed the structure, and the intensity of the characteristic fluorite peak decreased significantly, as can be seen by comparing Figs. 12a and 12b. This deformation has been reported to favour oxygen mobility, affecting the redox behaviour of the material [37]. The calcination temperature also affected the arrangement of atoms in the CeO₂ lattice (Fig. 12a), and the intensity of the Raman peak increased with calcination temperature due to the better arrangement of atoms. Raman characterisation also provided evidence of the improved thermal stability of the Ce–Zr mixed oxide. As shown in Fig. 12b, the intensities of the signals of Ce_{0.76}Zr_{0.24}O₂ calcined between 500 and 900 °C were about the same, and they increased slightly after calcination at 1000 °C. The shift of the Raman signal toward lower energies that occurred in Ce_{0.76}Zr_{0.24}O₂ calcined between 500 and 900 °C with regard to Ce_{0.76}Zr_{0.24}O₂-1000 is a sign of the improved oxygen mobility, which could be related to the presence of oxygen vacancies [38].

We investigated the redox properties of selected samples by H₂-TPR; the H₂ consumption profiles obtained are plotted in Fig. 13. H₂ consumption must be attributed to the reduction of

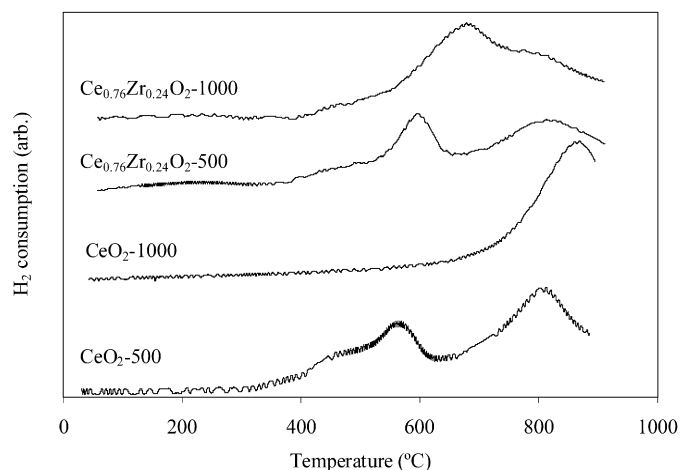


Fig. 13. H₂ consumption profiles during H₂-TPR for selected catalysts.

Ce⁴⁺ to Ce³⁺, because Zr⁴⁺ is a nonreducible cation. It is generally accepted [39] that two peaks characterise the reduction profile of pure CeO₂. The first peak, centred at around 500 °C in the profile of CeO₂-500, is attributed to the reduction of the uppermost layers of Ce⁴⁺; the second peak, centred at 800 °C, originated from the reduction of the bulk. The H₂ consumption profile of Ce_{0.76}Zr_{0.24}O₂-500 also had this shape, but the peak intensity ratio (surface/bulk reduction) was higher for the mixed oxide. This suggests enhanced oxygen mobility within the Ce_{0.76}Zr_{0.24}O₂ lattice compared with the bare CeO₂. On the other hand, a certain degree of inhomogeneous distribution of cerium and zirconium also can be inferred. A broad H₂ consumption band would be expected for a true Ce–Zr solid solution, where the surface and bulk reduction would occur concurrently, but a clear distinction between surface and bulk reduction would not be expected. Wu et al. [40] reported a bimodal H₂-TPR profile for a Ce_{0.5}Zr_{0.5}O₂ sample, which they ascribed to a possible “shell/core structure” concordant with a heterogeneous surface elemental distribution. These authors reported a surface Ce/Zr ratio of 1.3, higher than the nominal ratio (1.0) for this sample. The results of XPS analysis performed with our Ce_{0.76}Zr_{0.24}O₂ mixed oxide also showed a Ce/Zr ratio of 5.0, well above the value of 3.2 expected for this nominal composition. Along this line, Nagai et al. [41,42] also assessed (by XAFS) the Ce- and Zr-rich domains in a Ce_{0.5}Zr_{0.5}O₂ solid solution prepared by co-precipitation and subsequent calcination at 500 °C.

The profile of CeO₂-1000 contains only the bulk reduction peak, because of the very low BET surface area of this sample. The drastic effect of the calcination temperature on the surface redox properties of CeO₂ is not so obvious in Ce_{0.76}Zr_{0.24}O₂. The H₂ consumption profile of Ce_{0.76}Zr_{0.24}O₂-1000 shows a broad band instead of two well-defined peaks. The onset temperature of this band is consistent with a surface reduction process. The generally accepted explanation for this type of profile is that surface and bulk reduction occur concurrently [39]; that is, there is no clear distinction between the surface and bulk peaks, because oxygen located within the bulk comes to the surface as surface oxygen is consumed. This type of profiles is characteristic of materials with good oxygen mobility.

To summarise, the characterisation of CeO₂ and Ce_{0.76}Zr_{0.24}O₂ suggests that both materials have a fluorite structure, and that Ce–Zr incorporates Zr⁴⁺ cations into the CeO₂ framework. This incorporation of foreign cations enhances the thermal resistance of CeO₂, diminishing thermal sintering. As a consequence of this improved thermal resistance, Ce_{0.76}Zr_{0.24}O₂ calcined at high temperature has a greater BET surface area and better redox properties compared with pure CeO₂.

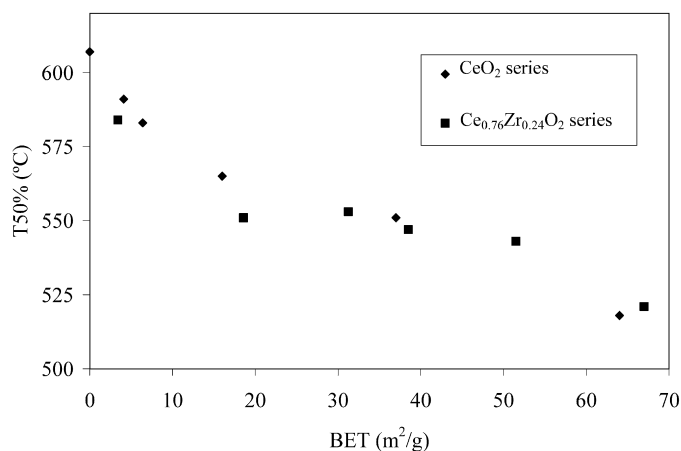


Fig. 14. T50% parameter versus BET surface area of catalysts (CeO₂-series and Ce_{0.76}Zr_{0.24}O₂-series).

It is not easy to distinguish between the relative contribution of structural properties (e.g., BET area; particle size) and other properties, such as redox behaviour or lattice oxygen mobility, in the catalytic activity toward soot combustion of CeO₂-based pure and mixed oxides. To gain insight into this distinction, Fig. 14 plots the temperature as a function of BET surface area for 50% soot conversion obtained from TPRs of the different CeO₂ and Ce_{0.76}Zr_{0.24}O₂ samples. A relationship between the parameters can be clearly seen, suggesting that the catalytic activity of pure CeO₂ and of the mixed oxide Ce_{0.76}Zr_{0.24}O₂ depends on surface area. A relationship between surface area and catalytic activity for soot oxidation in temperature-programmed oxidation by O₂, with soot and catalyst in tight contact, also has been also reported for the catalyst Ce_{0.95}Fe_{0.05}O_{1.975} [19]. This catalyst was calcined at different temperatures in the range of 500–750 °C, achieving surface areas of 92–10 m²/g. A linear correlation between surface area and activity was obtained for surface areas <40 m²/g, whereas the variation in activity was not so relevant for larger surface areas. In the present study, this threshold was not observed, probably because the soot and catalyst were in loose, not tight contact. For experiments in loose contact, we also would expect a threshold in surface area values above which the catalytic activity no longer improved; however, this limit seems to be above the maximum surface area reached in the current study (67 m²/g).

Despite the relationship between catalyst surface area and the T50% values obtained in the TPRs (Fig. 14), the isothermal reactions performed at 500 °C indicate that Ce_{0.76}Zr_{0.24}O₂-500 had better activity than CeO₂-500, and both samples had the same BET surface area. These differences can be attributed to the improved redox properties, deduced from H₂-TPR (Fig. 13), and/or enhanced lattice oxygen mobility, deduced from Raman spectroscopy (Fig. 12), of the mixed oxide. In conclusion, the structural properties of CeO₂-based pure and mixed oxides play important roles in the catalytic activity for soot oxidation, and other properties, such as redox behaviour and enhanced lattice oxygen mobility, also affect performance.

4. Conclusion

Based on our findings in the current study, we can conclude that the catalytic activity of CeO₂ for diesel-exhaust purification could be significantly improved by doping CeO₂ with Zr⁴⁺, with Ce_{0.76}Zr_{0.24}O₂ being the best formulation among those prepared and tested. This Ce–Zr mixed oxide had a slightly higher activity than bare CeO₂ for soot oxidation by NO_x/O₂ when both catalysts were calcined at 500 °C (with soot oxidation rates of 14.9 and 11.4 μg_{soot}/s, respectively, at 500 °C), and both catalysts exhibited

the same selectivity for CO₂ formation as a soot oxidation product. But Ce_{0.76}Zr_{0.24}O₂ showed enhanced thermal stability compared with pure CeO₂ (as deduced from XRD, Raman, TEM, N₂ adsorption and H₂-TPR characterisation), maintaining part of its activity for soot oxidation and selectivity toward CO₂ formation after calcination at temperatures as high as 1000 °C.

In addition, Ce_{0.76}Zr_{0.24}O₂ catalysed the reduction of NO_x by soot at around 500 °C more efficiently than CeO₂ did, thereby contributing to decreased NO_x emissions. The catalytic activity of CeO₂ and Ce_{0.76}Zr_{0.24}O₂ for soot oxidation by NO_x/O₂ depends on their textural properties (BET area; crystallite size), but other properties of the oxides, like redox behaviour and/or enhanced lattice oxygen mobility, play significant roles as well.

Acknowledgments

Financial support was provided by the Spanish Ministry of Education and Science (Project CTQ2005-01358) and the ABL contract funded by the Ramon y Cajal Program and the Generalitat Valenciana.

References

- [1] M.V. Twigg, *Appl. Catal. B* 70 (2007) 2.
- [2] J. Kašpar, P. Fornasiero, M. Graziani, *Catal. Today* 50 (1999) 285.
- [3] A. Trovarelli, *Catalysis by Ceria and Related Materials*, Catalytic Science Series, vol. 2, Imperial College Press, 2002, p. 281.
- [4] H.S. Gandhi, G.W. Graham, R.W. McCabe, *J. Catal.* 216 (2003) 433.
- [5] P. Fornasiero, G. Balducci, J. Kašpar, S. Meriani, R. di Monte, M. Graziani, *Catal. Today* 29 (1996) 47.
- [6] C.E. Hori, H. Permana, K.Y.S. Ng, A. Brenner, K. More, K.M. Rahmoeller, D. Belton, *Appl. Catal. B* 16 (1998) 105.
- [7] M. Daturi, E. Finocchio, C. Binet, J.C. Lavalley, F. Fally, V. Perrichon, H. Vidal, N. Hickey, J. Kašpar, *J. Phys. Chem. B* 104 (2000) 9186.
- [8] N. Hickey, P. Fornasiero, J. Kašpar, J.M. Gatica, S. Bernal, *J. Catal.* 200 (2001) 181.
- [9] G. Balducci, J. Kašpar, P. Fornasiero, M. Graziani, M. Saiful Islam, *J. Phys. Chem. B* 102 (1998) 557.
- [10] B.M. Reddy, P. Lakshmanan, P. Bharali, P. Saikia, G. Thirumurthulu, M. Muhler, W. Grulnert, *J. Phys. Chem. C* 111 (2007) 10478.
- [11] S. Eriksson, S. Rojas, M. Boutonnet, J.L.G. Fierro, *Appl. Catal. A* 326 (2007) 8.
- [12] D. Terribile, A. Trovarelli, C. de Leitenburg, A. Primavera, G. Dolcetti, *Catal. Today* 47 (1999) 133.
- [13] J.I. Gutiérrez-Ortiz, B. de Rivas, R. López-Fonseca, J.R. González-Velasco, *Appl. Catal. B* 65 (2006) 191.
- [14] F. Fally, V. Perrichon, H. Vidal, J. Kašpar, G. Blanco, J.M. Pintado, S. Bernal, G. Colon, M. Daturi, J.C. Lavalley, *Catal. Today* 59 (2000) 373.
- [15] I. Atribak, A. Bueno-López, A. García-García, *Catal. Commun.* 9 (2008) 250.
- [16] A. Bueno-López, K. Krishna, M. Makkee, J.A. Moulijn, *Catal. Lett.* 99 (2005) 203.
- [17] B.A.A.L. van Setten, M. Makkee, J.A. Moulijn, *Catal. Rev.* 43 (2001) 489.
- [18] J.P.A. Neeft, M. Makkee, J.A. Moulijn, *Fuel Proc. Technol.* 47 (1996) 1.
- [19] E. Aneggi, C. de Leitenburg, G. Dolcetti, A. Trovarelli, *Catal. Today* 114 (2006) 40.
- [20] A. Bueno-López, K. Krishna, M. Makkee, J.A. Moulijn, *J. Catal.* 230 (2005) 237.
- [21] K. Krishna, A. Bueno-López, M. Makkee, J.A. Moulijn, *Appl. Catal. B* 75 (2007) 189.
- [22] I. Atribak, I. Such-Basáñez, A. Bueno-López, A. García García, *J. Catal.* 250 (2007) 75.
- [23] A. Setiabudi, J. Chen, G. Mul, M. Makkee, J.A. Moulijn, *Appl. Catal. B* 51 (2004) 9.
- [24] K. Krishna, A. Bueno-López, M. Makkee, J.A. Moulijn, *Appl. Catal. B* 75 (2007) 201.
- [25] K. Krishna, A. Bueno-López, M. Makkee, J.A. Moulijn, *Appl. Catal. B* 75 (2007) 210.
- [26] M.L. Pisarello, V. Milt, M.A. Peralta, C.A. Querini, E.E. Miró, *Catal. Today* 75 (2002) 465.
- [27] B.A.A.L. van Setten, J.M. Schouten, M. Makkee, J.A. Moulijn, *Appl. Catal. B* 28 (2000) 253.
- [28] M. Adamowska, S. Muller, P. Da Costa, A. Krzton, P. Burg, *Appl. Catal. B* 74 (2007) 278.

- [29] M. Pijolat, M. Prin, M. Soustelle, O. Touret, P. Nortier, *J. Chem. Soc. Faraday Trans.* 91 (1995) 3941.
- [30] A. Setiabudi, M. Makkee, J.A. Moulijn, *Appl. Catal. B* 50 (2004) 185.
- [31] A. Bueno-López, A. García-García, J.A. Caballero-Suárez, *Environ. Sci. Technol.* 36 (2002) 5447.
- [32] A. Bueno-López, A. García-García, A. Linares-Solano, *Fuel Proc. Technol.* 77–78 (2002) 301.
- [33] D. Terribile, A. Trovarelli, J. Llorca, C. de Leitenburg, G. Dolcetti, *Catal. Today* 43 (1998) 79.
- [34] A. Nineshige, T. Taji, Y. Muroi, M. Kobune, S. Fujii, N. Nishi, M. Inaba, Z. Ogumi, *Solid State Ionics* 135 (2000) 481.
- [35] L.N. Ikryannikova, A.A. Aksenov, G.L. Markayan, G.P. Muravieva, B.G. Kostyuk, A.N. Kharlanov, E.V. Linina, *Appl. Catal. A* 210 (2001) 225.
- [36] M. Fernandez-García, A. Martínez-Arias, A. Iglesias-Juez, C. Belver, A.B. Hungria, J.C. Conesa, J. Soria, *J. Catal.* 194 (2000) 385.
- [37] P. Fornasiero, J. Kašpar, M. Grazini, *J. Catal.* 167 (1997) 576.
- [38] S. Rossignol, C. Descorme, C. Kappenstein, D. Duprez, *J. Mater. Chem.* 11 (2001) 2587.
- [39] G.L. Markaryan, L.N. Ikryannikova, G.P. Muravieva, A.O. Turakulova, B.G. Kostyuk, E.V. Lunina, V.V. Lunin, E. Zhilinskaya, A. Aboukais, *Colloids Surf. A* 151 (1999) 435.
- [40] W. Xiadong, L. Qing, W. Xiaodi, W. Duan, *J. Rare Earths* 25 (2007) 416.
- [41] Y. Nagai, T. Yamamoto, T. Tanaka, S. Yoshida, T. Nonaka, T. Okamoto, A. Suda, M. Sugiura, *J. Synchrotron Rad.* 8 (2001) 616.
- [42] Y. Nagai, T. Yamamoto, T. Tanaka, S. Yoshida, T. Nonaka, T. Okamoto, A. Suda, M. Sugiura, *Catal. Today* 74 (2002) 225.